One-dimensional particle simulation of wave propagation and generation of second harmonic waves in a composite of plasma and metamaterial

Akinori Iwai, Osamu Sakai, and Yoshiharu Omura

Citation: Physics of Plasmas **24**, 122112 (2017);
View online: https://doi.org/10.1063/1.5001108
View Table of Contents: http://aip.scitation.org/toc/php/24/12
Published by the American Institute of Physics

One-dimensional particle simulation of wave propagation and generation of second harmonic waves in a composite of plasma and metamaterial

Akinori Iwai,[1] Osamu Sakai,[2] and Yoshiharu Omura[1]
[1]*Research Institute for Sustainable Humanosphere, Kyoto University, Gokasho, Uji, Kyoto 611-0011, Japan*
[2]*Electronic Systems Engineering, The University of Shiga Prefecture, 2500 Hassakacho, Hikone, Shiga 522-8533, Japan*

(Received 22 August 2017; accepted 28 November 2017; published online 15 December 2017)

One-dimensional electromagnetic particle simulations are performed with the combination of the overdense plasma and the negative-permeability state (metamaterial). Transverse electromagnetic waves enter the plasma-metamaterial composite, and the waves propagate in it with a negative phase velocity and a positive group velocity. We confirm that the plasma-metamaterial composite has a negative refractive index. The dispersion relation of the composite has the propagation band under the plasma frequency, and we confirm this band by theoretical calculations with the kinetic effects and by particle simulations. When the phase velocity approaches the thermal velocity of the electrons, we find the damping of the transverse wave in the propagation band. The propagating transverse waves generate the propagating second harmonic waves throughout the composite. The intensities of the second harmonic waves are enhanced because the fundamental frequency waves are efficiently injected into the overdense plasma with the metamaterial since the refractive index is not imaginary but real with negative values. *Published by AIP Publishing.* https://doi.org/10.1063/1.5001108

I. INTRODUCTION

The propagation of electromagnetic waves in a plasma obeys various modes determined by plasma parameters and has been one of the important research topics in plasma physics.[1] Electrons and ions receive the forces of the incident electromagnetic waves, and their kinetics is determined by the equation of motion. Electric fields, the Lorentz force, and the interaction of particles are included as forces in the equation. When the amplitude of the incident wave is small, the wave propagates in a plasma with the dominant mode. As the amplitude increases, nonlinear harmonic waves are enhanced. The efficiency of the frequency conversion depends on the plasma parameters, and plasmas have been investigated as nonlinear optical materials with variable electric susceptibility.[2–5]

Plasmas are frequently-used tools for vapor deposition, surface treatment, and other industrial applications.[6] A plasma generated by microwaves is one of the typical schemes of the plasma discharge. When a microwave enters the room of the plasma discharge, the electron density n_e becomes larger than the cut-off density for the incident microwave, and a surface wave stands with the characteristic mode[7] between the entrance of the room and the high-n_e plasma (the overdense plasma). The surface wave sustains the overdense plasma, but the length of the generated plasma becomes short.

DC magnets or magnetic field coils are used to inject the energy of electromagnetic waves into the overdense plasma. The magnetized plasma has the propagation band under the electron cyclotron frequency, and we can optimize this frequency by the amplitude of the external DC magnets. This propagation mode is the Whistler mode, and a wavenumber becomes infinity when the incident wave frequency approaches the electron cyclotron frequency. The electron cyclotron resonance (ECR) heating is useful for the efficient power injection into the overdense plasma,[6] but it is difficult to prepare a large-scale DC magnet for the plasma generation systems.

Metamaterials are artificial composites made of unit patterns whose size is much smaller than the wavelength of the corresponding waves. Metamaterials give the extraordinary propagation of electromagnetic waves and it cannot occur in natural materials. Refractive index N becomes negative in metamaterials because both permittivity ε and permeability μ become negative.[9] Wave propagation in negative N was simulated and analyzed theoretically.[10–12] Generation of the second harmonic waves in negative N with quadratic nonlinear response was reported,[12,13] and nonlinear frequency conversion process was shown to be similar to that in typical nonlinear optics.[14] The experimental verification was performed with the combination of the split-ring resonators (SRRs) as negative-μ metamaterials[8] and the array of metal wires as a negative-ε material.[15–17] This array of metal wires has the cut-off frequency and obtains a negative ε under this frequency as in an overdense plasma.[18]

A combination of an overdense plasma and a negative-μ metamaterial has been studied in experiments[19–21] and in simulations.[22,23] Although Iwai *et al.* showed that the estimated N was negative, the second harmonic wave was enhanced,[20] and SRRs had electric connection with plasma microscopically,[21] wave propagation is not clarified in the composite of an overdense plasma and a negative-μ metamaterial. Sakai[22] performed FDTD simulations and reported the wave propagation with a negative N in the array of plasma columns under a negative-μ state. Kourtzanidis *et al.*[23] clarified the local electromagnetic fields around an SRR when a plasma exists near the SRR. Since both reports used the fluid model to simulate plasmas, nonlinear and kinetic effects of a plasma were not considered. These effects must be included

in a case that a high-power electromagnetic wave enters the overdense plasma under a negative-μ state.

In this paper, we perform particle simulations in a negative-μ state to clarify the propagation of electromagnetic waves in the composite of the overdense plasma and the negative-μ metamaterial (the plasma-metamaterial composite) including nonlinear and kinetic effects of the plasma, and use the electromagnetic particle code modified from KEMPO1.[24,25] In Sec. II, we show the simulation model and the method to deal with the negative-μ metamaterial. In Sec. III, we show the propagation of electromagnetic waves, the propagation mode, and the efficient generation and propagation of the second harmonic waves in the plasma-metamaterial composite. Finally, we give a summary in Sec. IV.

II. SIMULATION MODEL

References 24 and 25 describe the calculation scheme and many examples of simulation results by KEMPO1. We add the magnetic current in KEMPO1 to simulate a metamaterial effect[10,22] and describe this modification in detail using Eqs. (3) and (4). Figure 1 shows the simulation model. An external current $\boldsymbol{J}_s$ exists at $x = -12.8$ and oscillates along the z axis, $\boldsymbol{J}_s = \hat{z}J_z = \hat{z}J_0 \sin(\omega_0 t)$ where $\hat{z}$ is a unit vector along the z axis. The electromagnetic wave is radiated from this external current and propagates along the x axis. The wave consists of the z-axis component of the electric field $\boldsymbol{E}$, E_z, and the y-axis component of the magnetic flux $\boldsymbol{B}$, B_y. The plasma-metamaterial composite exists in the region where $0 \le x \le 12.8$, and we call the region as the plasma region.

When the radiated wave enters the plasma region, electrons and ions oscillate and generate true charge current $\boldsymbol{J}_p$. The current density $\boldsymbol{J}_p$ is determined by velocities of all particles $\boldsymbol{v}_s$ and the dielectric response of the plasma is expressed as follows:

$$\nabla \times \boldsymbol{B} = \mu_0 \boldsymbol{J}_p + \mu_0 \varepsilon_0 \frac{\partial}{\partial t}\boldsymbol{E}, \tag{1}$$

$$\frac{\mathrm{d}}{\mathrm{d}t}(\gamma \boldsymbol{v}_s) = \frac{q_s}{m_s}(\boldsymbol{E} + \boldsymbol{v}_s \times \boldsymbol{B}), \tag{2}$$

where μ_0 is the permeability in vacuum, ε_0 is the permittivity in vacuum, γ is the Lorentz factor, and q_s and m_s are the charge and rest mass of a particle "s." In this simulation, γ is calculated for all particles because some electrons become energetic ones.

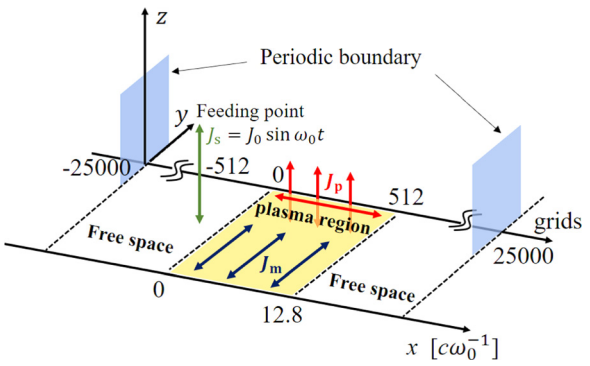

FIG. 1. The one-dimensional model of the composite of the plasma and the metamaterial. The current source J_s at $x = -12.8$ radiates electromagnetic waves along the x axis. The plasma and the metamaterial exist only in $0 \le x \le 12.8$, and both sides, $x < 0$ and $12.8 < x$, are free space.

When the incident amplitude of the wave is small, the plasma has the simple dispersive reaction to $\boldsymbol{E}$ as $\partial \boldsymbol{J}_p/\partial t \sim \omega_p^2 \boldsymbol{E}$ where ω_p is the plasma frequency. The left term is equal to the right term when the plasma consists of cold particles.

The metamaterial used in the experiments[20,21] reacts to the penetrating $\boldsymbol{B}$ and obtains the magnetic resonance. This magnetic reaction of the metamaterial is complementary to the electric reaction of the plasma, and we can assume a magnetic current $\boldsymbol{J}_m$ as the magnetic reaction of the metamaterial in a classical approach.[10,22] When it is assumed that this magnetic dispersive reaction is expressed as the Drude type dispersion and does not depend on the amplitude of $\boldsymbol{B}$, we can rewrite the Maxwell equations as

$$\nabla \times \boldsymbol{E} = -\boldsymbol{J}_m - \frac{\partial}{\partial t}\boldsymbol{B}, \tag{3}$$

$$\frac{\partial}{\partial t}\boldsymbol{J}_m = \omega_m^2 \boldsymbol{B}, \tag{4}$$

where ω_m is the magnetic resonance frequency. The modified point of this code from KEMPO1 is insertion of $\boldsymbol{J}_m$. The metamaterial effect based on $\boldsymbol{J}_m$ is not affected by $\boldsymbol{E}$ and plasmas in this simulation. $\boldsymbol{J}_m$ is determined only by $\boldsymbol{B}$ and the constant ω_m.

The current density $\boldsymbol{J}_p$ includes linear, nonlinear, and kinetic motions of the particles and consists of the x- and z-axis components. The magnetic current density $\boldsymbol{J}_m$ is parallel to $\boldsymbol{B}$ and consists of the y-axis component. The effective permittivity of the plasma ε_p and the effective permeability of the metamaterial μ_m are expressed as follows: $\varepsilon_p \sim 1 - \omega_p^2/\omega^2$ and $\mu_m = 1 - \omega_m^2/\omega^2$.

Both sides of the plasma region are set as free space, and we call the side where $x < 0$ and $12.8 < x$ as the upstream side and the downstream side, respectively. Boundaries of the simulation system are defined as periodic

TABLE I. Parameters of 1D-PIC simulation.

Parameters	value
Grid spacing Δx	0.5
Number of grids	50 000
System length	50 000
Length of plasma region	512
Time Steps Δt	0.02
Light speed c	20
Incident wave frequency ω_0	1.0
Electron plasma frequency ω_{pe}	1.5
Ion plasma frequency ω_{pi}	0.015
Magnetic resonance frequency ω_m	1.7
Charge to mass ratio of on electron	−1.0
Charge to mass ratio of an ion	0.0001
Thermal velocity of electrons v_{the}	0.75
Thermal velocity of ions v_{thi}	0.0075
Number of electrons	131 072
Number of ions	131 072
Amplitude of current source J_0	100

boundaries to satisfy the continuity of particles in this simulation space, which is large enough to neglect the waves coming from the boundaries in this calculation time.

Table I shows the parameters in this simulation. The speed of light c is set at 20 to satisfy Courant condition because $\Delta x/\Delta t = 25$. The frequency of the incident external current ω_0 is set at 1.0, and the electron plasma frequency ω_{pe} and the magnetic resonance frequency ω_m are set at $1.5\omega_0$ and $1.7\omega_0$, respectively, to simulate the negative-ε overdense plasma and the negative-μ metamaterial, respectively. The mass ratio between an electron and an ion is 0.0001 to assume heavy ions, and they hardly move. The numbers of electrons and ions are 256 particles in one grid, and they exist in the plasma region at equal intervals. The energy distribution function is the Maxwellian distribution for both electrons and ions. The electron thermal velocity v_{the} determines the Debye length $\lambda_D = v_{the}/\omega_{pe}$, and we set v_{the} as small as possible under the condition that $\lambda_D \geq 0.5\Delta x$. Parameters for ions ω_{pi} and v_{thi} are set as 0.01 ω_{pe} and 0.01 v_{the}. Heavy ions hold electrons within the plasma region and sustain the state of a bulk plasma.

III. SIMULATION RESULTS

A. Wave propagation in a plasma-metamaterial composite

Figure 2 shows the time development of E_z in cases with various combinations of ω_{pe}, ω_{pi}, and ω_m. Figure 2(a) shows that E_z propagates with the light velocity c downstream in free space (ω_{pe}, ω_{pi}, and ω_m are 0.0). The gradient of an equiphase line is 1 because variable x on the x axis is normalized by $c\omega_0^{-1}$ and t in the y axis is normalized by ω_0^{-1}. The amplitude of E_z in free space can be calculated as follows:[26]

$$|E_z| \equiv E_{z0} = \frac{1}{2} c\mu_0 J_0. \tag{5}$$

In Fig. 2, the amplitude of E_z is normalized by E_{z0}.

The wave incidence into the metamaterial is simulated, and the result is shown in Fig. 2(b). The value of permeability $\mu_m(\omega_0)$ becomes -1.9, which is similar to μ of our experimental SRRs.[20] The radiated wave from the current source reaches the entrance of the plasma region at $t = 12.8$, and it is reflected. The radiated wave and the reflected wave create a standing wave in the upstream side ($-12.8 \leq x < 0$). The impedance of the plasma region Z_p can be calculated as $\sqrt{\mu(\omega_0)} = \sqrt{(\omega_0^2 - \omega_m^2)/\omega_0^2}$ for the incident wave. The value of impedance Z_p becomes a pure imaginary, and the plasma region works like as a perfect reflector.

We set $\omega_{pe} = 1.5\omega_0$ and $\omega_{pi} = 0.015\omega_0$ to simulate the overdense plasma. Figure 2(c) shows the time development of E_z, and it is similar to that in the metamaterial in Fig. 2(b). The impedance of the overdense plasma can be calculated as $Z_p = \sqrt{1/\varepsilon_p(\omega_0)} \sim \sqrt{\omega_0^2/(\omega_0^2 - \omega_{pe}^2)}$ (cold plasma assumption), and becomes a pure imaginary value too. The sign of Z_p in the overdense plasma is opposite to that in the metamaterial, and the standing wave in the upstream side includes a π-phase shift between Figs. 2(b) and 2(c).

Setting $\omega_{pe} = 1.5\omega_0$, $\omega_{pi} = 0.015\omega_0$, and $\omega_m = 1.7\omega_0$, we simulated the propagation of the wave in the plasma-metamaterial composite. In Fig. 2(d), most parts of the incident wave penetrate into the plasma region after $t = 12.8$. This transmitted wave propagates in the plasma region downstream with a velocity less than c and keeps its wave shape in the plasma region. This wave is not an evanescent wave and has a finite wavenumber k. Reflection from the plasma region occurs slightly because $Z_p \sim \sqrt{\mu_m(\omega_0)/\varepsilon_p(\omega_0)}$, and it is slightly different from the impedance in free space. An 1D FDTD simulation in the case with negative μ and ε was performed in Ref. 10, and a pulse wave penetrated into the double-negative region, although it was reflected in cases with a negative μ or negative ε. This result fairly well matches with Fig. 2 in this particle simulation. This agreement with Ref. 10 stresses that negative N is realized by the combination of charged particles and a metamaterial based on classical approach with magnetic current $\boldsymbol{J}_m$.

Since an equiphase line in the plasma region has a negative slope, the propagating wave has a negative phase velocity v_{ph}. The downstream propagation of the wavefront implies that the electromagnetic energy is transported downstream, and the group velocity has a *positive* value. Agranovich *et al.* calculated the group velocity in the negative N region and showed that it became negative in Ref. 12. This indication seems to contradict with Fig. 2(d). However, a negative group velocity means that the direction of group velocity is opposite to that of wavenumber vector, and this relation of wavenumber vector (phase velocity) and group velocity in our results is the same as that reported in Ref. 12.

We performed the Fast Fourier transform (FFT) for the time development of E_z over a period of $128 \leq t \leq 297.44$ (=15 000 Δt, end of these simulations) and Fig. 3 shows the frequency spectra of E_z as a function of x in (a) free space, (b) the metamaterial, (c) the overdense plasma, and (d) the plasma-metamaterial composite.

A sharp spectrum exists only at $\omega = \omega_0$ in Fig. 3(a) since the radiated wave propagates in free space. The standing wave in the upstream side and the evanescent wave in the plasma region are shown in Figs. 3(b) and 3(c) as the spectrum at $\omega = \omega_0$. The magnetic resonance occurs in the metamaterial at ω_m, and a small peak at $\omega_m (= 1.7\omega_0)$ is shown in Fig. 3(b). In Fig. 3(c), the electrons oscillate with ω_{pe}, and we observe a peak at $\omega_{pe} (= 1.5\omega_0)$.

Figure 3(d) shows a sharp and strong peak at $\omega = \omega_0$ in the upstream side, the plasma region, and the downstream side like Fig. 3(a). Spectra emerge under $1.5\omega_0$, and it seems that this frequency range becomes the propagation band. A weak spectrum is seen at $\omega = 3.0\omega_0$ and it is considered as the third harmonic wave from a nonlinear interaction between electrons and waves. This nonlinear interaction is explained in Sec. III C.

B. Dispersion relation of a plasma-metamaterial composite

When the plasma has cold electrons and v_{the} is small enough, $\varepsilon_p(\omega) = 1 - \omega_{pe}^2/\omega^2$, and we have the analytical form of the dispersion relation for the composite of the cold plasma and the metamaterial as follows:

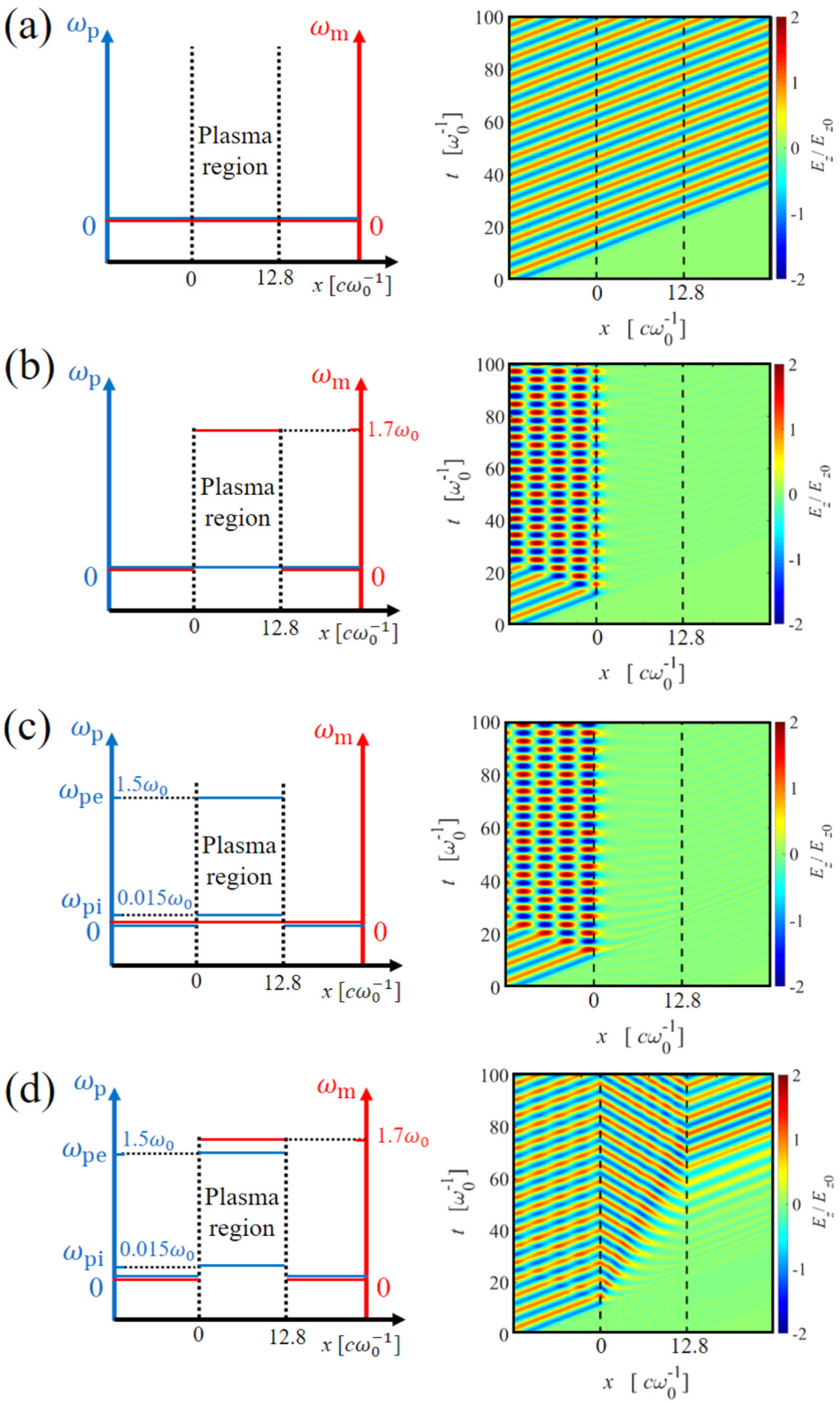

FIG. 2. The transverse component of the electric field E_z around the plasma region ($0 \le x \le 12.8$) from $t = 0$ to $100\,\omega_0^{-1}$. The plasma region has different conditions. (a) free space, (b) the metamaterial, (c) the overdense plasma, and (d) the plasma-metamaterial composite. The electric field is normalized by E_{z0}, which is an amplitude in free space when $J_s = J_0$.

$$ck = \omega\sqrt{1-\frac{\omega_{pe}^2}{\omega^2}}\sqrt{1-\frac{\omega_m^2}{\omega^2}}. \tag{6}$$

In the particle simulation of high frequency electromagnetic waves, we can neglect the motions of heavy ions, focusing on the kinetic motions of electrons and the interaction between electrons and waves.

Taking into account the kinetic effects of electrons,[27] we obtain the dispersion relation of the composite of the hot isotropic plasma and the metamaterial as follows:

$$c^2k^2 = \omega^2 - \omega_m^2 + \omega_{pe}^2\left(1-\frac{\omega_m^2}{\omega^2}\right)\left(j\sqrt{\pi}Ce^{-C^2} - I_1\right), \tag{7}$$

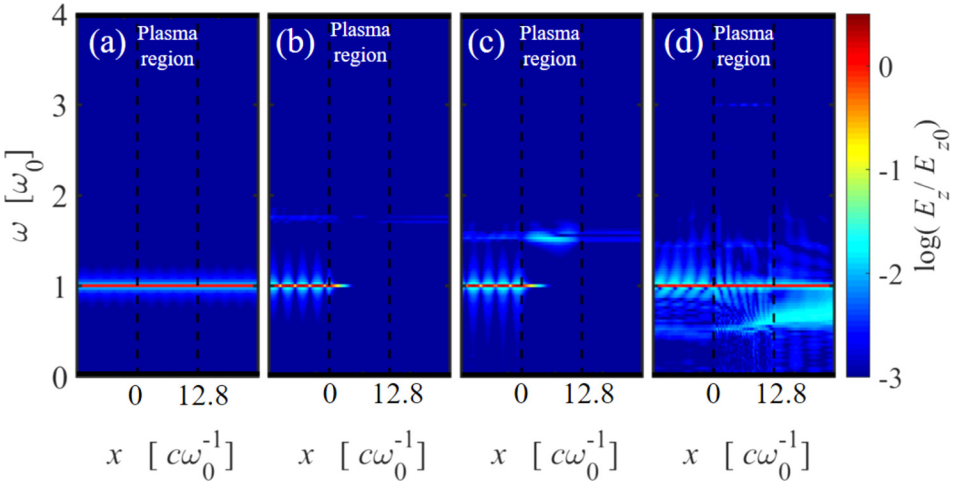

FIG. 3. Frequency spectra of E_z as a function of x in four cases of Fig. 2. The Fourier transform of E_z is performed over a period of $128 \le t \le 297.44$.

$$C = \frac{\omega}{\sqrt{2}v_{\mathrm{the}}}, \tag{8}$$

$$I_1 = 1 - \mathrm{e}^{-C^2} + \sum_{n=1}^{\infty} \frac{(2n-1)!!}{2^n n!} \left[\frac{n!}{C^{2n}} - \mathrm{e}^{-C^2} \times \left\{ 1 + \frac{n}{C^2} + \frac{n(n-1)}{C^4} + \cdots \frac{n!}{C^{2n}} \right\} \right], \tag{9}$$

where $(2n-1)!!$ is defined as $(2n-1)!! \equiv (2n-1)\cdot(2n-3)\cdots 3\cdot 1$ and $\mathrm{j} = \sqrt{-1}$. Equation (7) includes an imaginary term, and k becomes a function of complex $\omega = \omega_{\mathrm{r}} + \mathrm{j}\omega_{\mathrm{i}}$, where ω_{r} and ω_{i} are the real and imaginary parts of ω, respectively, and ω_{i} indicates a time variation of the amplitude of waves. We solve Eq. (7) numerically with variables k, ω_{r}, and ω_{i}.

Figure 4(a) shows the dispersion relations from Eqs. (6) (dotted line: the cold plasma) and (7) (circles: the hot isotropic plasma). The parameters c, ω_{pe}, ω_{m}, and v_{the} were set as in Table I. We included the expansion term I_1 up to $n = 3$. When $\omega > 0.6\omega_0$, the dispersion relation of the hot isotropic plasma shows good agreement with that of the cold plasma. The imaginary part $\omega_{\mathrm{i}} = 0$ and the kinetic motions of electrons hardly affect the propagation of waves in this frequency range.

When $\omega \le 0.6\omega_0$, $|k|$ in the case with the hot plasma becomes larger than that of the cold plasma and ω_{i} emerges and rapidly decreases. Since v_{ph} approaches v_{the} in this frequency range, ω_{i} has negative values, and a damping is caused. Since $\omega_{\mathrm{i}} = 0$ at every frequency [the dotted line in Fig. 4(a)], the damping derived from ω_{i} cannot occur in the cold plasma case. In a general non-magnetized plasma, the Landau damping occurs only in the interaction between electrons and *longitudinal* waves of electric fields because transverse waves absolutely have v_{ph} greater than c.[27] In the composite of the hot isotropic plasma and the metamaterial, v_{ph} becomes small enough, and we can observe the damping in the mode of the *transverse* waves.

We applied the FFT to E_z in space and time in the plasma region when $J_{\mathrm{s}} = 0.0$. We draw ω–k diagrams in cases with and without the metamaterial. The kinetic motions of electrons radiate electromagnetic waves including some frequencies even if there is no external incidence of waves, and the wave with ω propagates in the plasma region with the wavenumber k as a function of ω. The resultant ω–k diagram has peaks on the dispersion relation of the plasma region.

Figure 4(b) shows the ω–k diagram for the plasma without the metamaterial. The dotted line is the analytical dispersion relation of the cold plasma $ck = \omega\sqrt{1 - \omega_{\mathrm{pe}}^2/\omega^2}$ and this diagram perfectly corresponds to the analytical solution. Since $v_{\mathrm{the}}/c = 0.0375$ and velocities of electrons v_{se} have Maxwellian distribution, v_{se}/c is distributed from 0 to ~0.1. In Figs. 4(b) and 4(c), white triangles show the area with v_{ph} being less than 0.1, and the thermal noise of electrons is

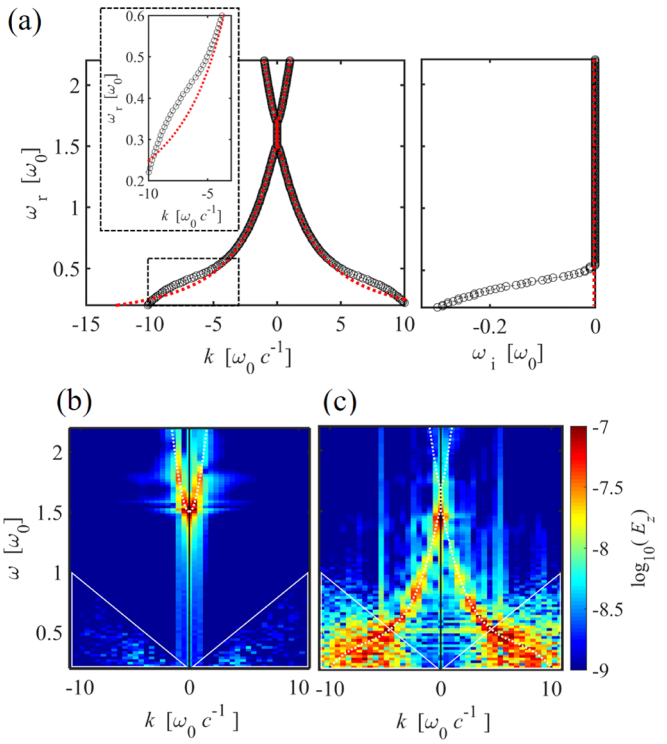

FIG. 4. The dispersion relation for the plasma-metamaterial composite in which the electric and magnetic resonance frequencies ω_{pe} and ω_{m} are $1.5\omega_0$ and $1.7\omega_0$, respectively. (a) The numerical solution of the wavenumber k as a function of the complex frequency $\omega = \omega_{\mathrm{r}} + \mathrm{j}\omega_{\mathrm{i}}$ in the case of hot isotropic plasma. The dotted line shows the case of the cold plasma. The box of the dash line indicates the enlarged area, $0.2 \le \omega_{\mathrm{r}} \le 0.6$. The ω-k diagrams in (b) the overdense plasma, and (c) the plasma-metamaterial composite. The white triangle shows an area with v_{ph} is less than 0.1.

found in these triangles. Intensity of the thermal noise is much smaller than that of the spectra on the dispersion curve in Fig. 4(b), and we do not find any kinetic effects of electrons for the transverse waves in the ordinary plasma.

The ω–k diagram of the plasma-metamaterial composite is shown in Fig. 4(c). The dotted line is the calculated dispersion relation in the hot isotropic plasma case by Eq. (7). Intensities of spectra in $\omega \leq 1.5\omega_0$ are emphasized. In the range where $0.6\omega_0 < \omega \leq 1.5\omega_0$, peaks of spectra correspond to the dispersion relation calculated from Eq. (7) in Fig. 4(a). When $\omega \leq 0.6\omega_0$, the spectra enter the inside of the triangle area and are mixed with the thermal noise of electrons since v_{ph} comes to be less than 0.1. The intensity of the noise is clearly stronger than that in Fig. 4(b), though there is no external incidence of waves since radiated waves in $\omega < 0.6\omega_0$ have v_{ph} being close to v_{se} and transfer their energy to electrons. This enhanced thermal noise shows the damping of transverse waves and the ω–k diagram in Fig. 4(c) shows good agreement with the calculated dispersion relation including ω_i in Fig. 4(a).

Figures 5(a) and 5(b) show the group velocity v_g and v_g^{-1} in the composite with the cold plasma (the dotted line) and with the hot isotropic plasma (the circles). The dotted line is given as the analytical solution by performing $v_g = \partial\omega/\partial k$ for Eq. (6). When we performed the numerical calculation for Eq. (7), ω_r and k have discrete values with $0.01\omega_0$- and $0.002\omega_0 c^{-1}$-intervals. In the hot plasma case, v_g is defined as the difference between next symbols, (e.g., $v_g(\omega_1)$ is defined as $v_g(\omega_1) = 0.01/\{k(\omega_1 + 0.01) - k(\omega_1)\}$), and v_g comes to have discrete values.

When $\omega > 0.6\omega_0$, v_g in the composite with the hot isotropic plasma corresponds to that in the case with the cold plasma. The group velocity v_g increases as ω increases, and it rapidly decreases as ω approaches ω_{pe}. $v_g \sim c(1 + \omega_{pe}^2/\omega^2)^{-1}$ in the case that $\omega_{pe} = \omega_m$ in Ref. 10 and v_g has a finite value when $\omega = \omega_{pe}$. In this simulation, v_g rapidly approaches 0 when ω is close to ω_{pe} in Fig. 5(a) because $\omega_{pe} \neq \omega_m$. The group velocity v_g in the hot-plasma case is slightly smaller than that in the cold-plasma case around $0.5\omega_0$, and it has the minimum value when $\omega \sim 0.4\omega_0$. The inversed value v_g^{-1} indicates the time that a wave with ω requires for propagating within a certain length.

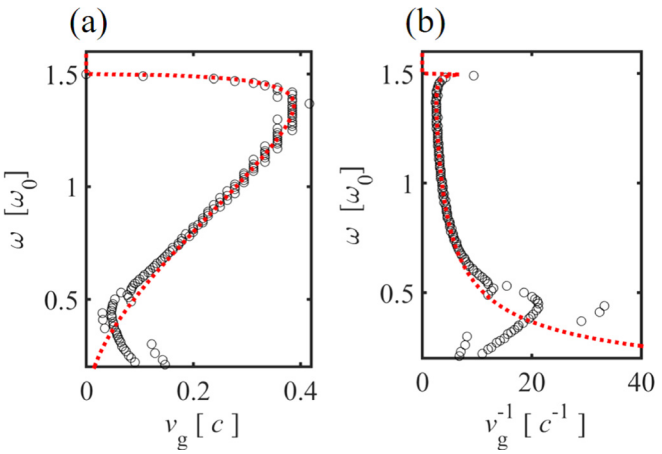

FIG. 5. (a) The calculated group velocity v_g as a function of frequency ω. The dotted curve shows the analytical solution in the case of the cold plasma. The circles indicate the case of the hot plasma. (b) v_g^{-1} as a function of ω.

In Fig. 2(d), we found the propagation of waves with different v_{ph} and v_g when the wavefront entered the composite. In order to confirm that the dispersion of the wavefront obeys the dispersion relation calculated in Eq. (7), we performed the short time fast Fourier transform (STFFT)[28] for the time development of E_z in the composite. When $f(t)$ expresses E_z at a position as a function of time, we multiplied a window function $w(t)$ with $f(t)$ and applied the FFT to $f(t) \cdot w(t - t_0)$. We used the Hann window, $w(t) = 0.5 - 0.5\cos(2\pi t/l_w)$ $(0 \leq t \leq l_w)$ and l_w is the length of this window. In this STFFT, we set $l_w = 81.92\,\omega_0^{-1}$ $(= 1024\Delta t)$ and swept t_0. We obtained the frequency spectra at $t = t_0 + l_w/2$ by the FFT for $f(t) \cdot w(t - t_0)$.

Figure 6 shows the time development of frequency spectra of E_z at $x = 2.5$, 5.0, 7.5, 10.0, and 12.5. We set plasma parameters as in Table I, and the external current is set as $J_s = 2J_0$. The intensity of the spectra in Fig. 6 shows the normalized value $E_z/2E_{z0}$ where E_{z0} is calculated using Eq. (5). The arrival timing of the wavefront is delayed as the position of the observation becomes farer from the entrance. The white points in Fig. 6 express a theoretical arrival timing of waves as a function of ω and is calculated as $12.8 + x/v_g(\omega)$. These points correspond to the timing when the peaks of spectra emerge when $0.6\omega_0 < \omega$. In the composite, a band gap exists in $1.5\ \omega_0 \leq x \leq 1.7\omega_0$. The spectra in the band gap decrease as the increment of x, and the waves in the band gap becomes evanescent waves. In all positions, spectra in $\omega < 0.5\omega_0$ are not observed. In Fig. 4, waves in $\omega < 0.6\omega_0$ are hard to propagate into the composite with the hot isotropic plasma because of ω_i damping. In the cold plasma case, propagation of waves should occur in all frequencies except the band gap. The spectra in Fig. 6 clearly show a lower band gap in $\omega < 0.5\omega_0$, and Fig. 6 matches the hot isotropic plasma case.

C. Generation of second harmonic waves in a plasma-metamaterial composite

1. Analysis model

We introduce an analytical model of second harmonic generation before discussion of results in the particle simulations. Referring to Ref. 29, we calculate the intensity of the second harmonic wave in E_x with the perturbation method. When we deal with the plasma in the composite as cold electron fluid, we can introduce the momentum balance equation to determine a motion of electrons

$$d\boldsymbol{u}_e/dt = -e/m_e(\boldsymbol{E} + \boldsymbol{u}_e \times \boldsymbol{B}), \tag{10}$$

where $\boldsymbol{u}_e$ is the averaged velocity of electrons, e is a charge of an electron, and m_e is a mass of an electron. Lorentz factor γ in Eq. (2) can be omitted because we consider a cold electron plasma, and energy of electrons is small enough to assume that $\gamma = 1$.

When $\boldsymbol{u}_e$, $\boldsymbol{E}$, and $\boldsymbol{B}$ are expanded as a function of $\exp\{j(\boldsymbol{k}_n \cdot \boldsymbol{x} - n\omega_0 t)\}$, where n is a positive integer from 1

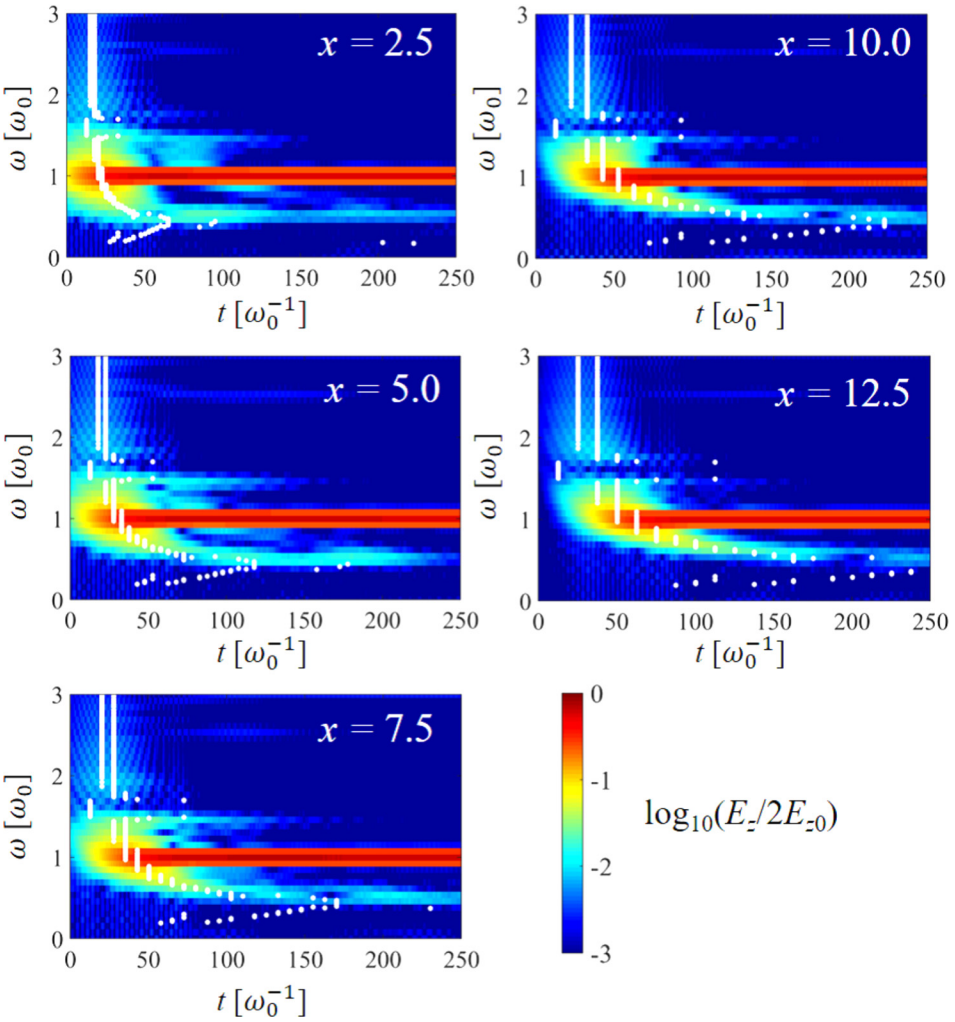

FIG. 6. The time development of the frequency spectra for the transverse component E_z from $x = 15$ to 25 when $J_s = 2J_0$. The white points indicates the calculated delay time.

to infinity and $\boldsymbol{k}_n$ is the wavenumber vector at $\omega = n\omega_0$, they can be expressed as

$$\boldsymbol{u}_e = \sum_{n=1}^{\infty} \boldsymbol{u}_{en} \exp\{\mathrm{j}(\boldsymbol{k}_n \cdot \boldsymbol{x} - n\omega_0 t)\}, \tag{11}$$

$$\boldsymbol{E} = \sum_{n=1}^{\infty} \boldsymbol{E}_n \exp\{\mathrm{j}(\boldsymbol{k}_n \cdot \boldsymbol{x} - n\omega_0 t)\}, \tag{12}$$

$$\boldsymbol{B} = \sum_{n=1}^{\infty} \boldsymbol{B}_n \exp\{\mathrm{j}(\boldsymbol{k}_n \cdot \boldsymbol{x} - n\omega_0 t)\}, \tag{13}$$

where the subscript n expresses the oscillation at $\omega = n\omega_0$. Substituting Eqs. (11)–(13) to Eq. (10), we can substitute $\partial/\partial t$ and ∇ with $-nj\omega$ and $j\boldsymbol{k}_n$, respectively. When we focus on components at $n = 1$, the left- and right-hand sides in Eq. (10) are $-j\omega_0 \boldsymbol{u}_{e1} + (\boldsymbol{u}_{e1} \cdot j\boldsymbol{k}_1)\boldsymbol{u}_{e1}$ and $-e/m_e(\boldsymbol{E}_1 + \boldsymbol{u}_{e1} \times \boldsymbol{B}_1)$. Since the incident wave propagates along the x axis in this simulation, the second term in the left-hand side comes to be 0. Selecting the components at $\omega = \omega_0$ because $\boldsymbol{u}_{e1} \times \boldsymbol{B}_1$ comes to be an amplitude in the form of $\exp\{2j(\boldsymbol{k}_1 \cdot \boldsymbol{x} - \omega t)\}$, we obtain $\boldsymbol{u}_{e1}$ as

$$\boldsymbol{u}_{e1} = \frac{e}{j\omega m_e}\boldsymbol{E}_1. \tag{14}$$

In the fluid model, we can express the current flux $\boldsymbol{J}_p = -en_e\boldsymbol{u}_e$ where n_e is electron density. The Lorentz force between $\boldsymbol{u}_{e1}$ and $\boldsymbol{B}_1$ creates a current oscillating at $\omega = 2\omega_0$, and we can introduce current flux at $\omega = 2\omega_0$ $\boldsymbol{J}_{p2}$ as

$$\boldsymbol{J}_{p2} = -\frac{e^2 n_e}{j2\omega m_e}(\boldsymbol{u}_{e1} \times \boldsymbol{B}_1). \tag{15}$$

A slight fluctuation of charge density at $\omega = 2\omega_0$ ρ_2 occurs by $\boldsymbol{J}_{p2}$ with obeying the equation of continuity $-\partial\rho_2/\partial t = \nabla \cdot \boldsymbol{J}_{p2}$. Combining this equation with the Gauss's low $\nabla \cdot \boldsymbol{E}_2 = \rho_2/\varepsilon_0$, we obtain $\nabla \cdot (\partial \boldsymbol{E}_2/\partial t + \boldsymbol{J}_{p2}/\varepsilon_0) = j\boldsymbol{k}_2 \cdot (\partial \boldsymbol{E}_2/\partial t + \boldsymbol{J}_{p2}/\varepsilon_0) = 0$. The second order vectors $\boldsymbol{J}_{p2}$, $\boldsymbol{E}_2$, and $\boldsymbol{k}_2$ are along the x axis and we obtain

$$\boldsymbol{E}_2 = -j\frac{1}{2\omega\varepsilon_0}\boldsymbol{J}_{p2}. \tag{16}$$

In this simulation, $\boldsymbol{u}_{e1}$ and $\boldsymbol{E}_1$ are along the z axis, $\boldsymbol{B}_1$ is along the y axis, and $\boldsymbol{J}_{p2}$ and $\boldsymbol{E}_2$ are along the x axis. Substituting Eq. (14) into (15) and Eq. (15) into Eq. (16), we obtain the intensity of the second harmonic wave

$$E_{x2\omega_0} = -j\frac{1}{4}\left(\frac{\omega_{pe}^2}{\omega^2}\right)^2 \frac{e}{m_e\omega} E_{z1}B_{y1}, \tag{17}$$

$$= -\mathrm{j}\frac{1}{4}\left(\frac{\omega_{\mathrm{pe}}^2}{\omega^2}\right)^2 \frac{e}{m_{\mathrm{e}}\omega c}\sqrt{\frac{\omega^2-\omega_{\mathrm{pe}}^2}{\omega^2-\omega_{\mathrm{m}}^2}}E_{z1}^2, \tag{18}$$

where we rewrite $\boldsymbol{E}_1$, $\boldsymbol{E}_2$, and $\boldsymbol{B}_1$ as E_{z1}, E_{2x}, and B_{y1}, respectively.

2. Second harmonic waves in particle simulations

The Lorentz force term $\boldsymbol{v}_{\mathrm{s}} \times \boldsymbol{B}$ in Eq. (2) can create harmonic oscillation waves, and they are perpendicular to $\boldsymbol{v}_{\mathrm{s}}$ and $\boldsymbol{B}$. The incident E_z oscillates electrons with $\omega = \omega_0$, and v_z also has the oscillation component with ω_0. The Lorentz force between v_z and B_y gives the second harmonic components to the longitudinal wave E_x.

In this simulation, E_x is calculated by Gauss's law, and E_x fluctuates only in the plasma region with charged particles. We applied the FFT to E_x over a period of $128 \le t \le 297.44$ when $J_s = 2J_0$. Figure 7(a) shows the frequency spectra of E_x in the overdense plasma. The intensity of E_x is normalized by $2E_{z0}$. The incident wave cannot propagate into the overdense plasma and penetrates up to the skin depth [Fig. 3(c)]. The generated second harmonic wave becomes an evanescent wave and it is limited near the entrance. The second harmonic wave moves electrons, and the spatial profile of electrons fluctuates slightly. This fluctuation slightly enhances the electron plasma wave ($\omega = 1.5\omega_0$), and it propagates in the plasma region.

We applied the inverse FFT to the spectra of E_x with the frequency filter at $\omega = 2\omega_0$ and obtain the time development of E_x at $\omega = 2\omega_0$. Figure 7(a) shows E_x at $\omega = 2\omega_0$ in $200 \le t \le 250$ in the overdense plasma, and it becomes an evanescent wave.

Figure 7(b) shows the case of the composite. A spectrum at $\omega = 2\omega_0$ keeps a strong intensity at every position in the plasma region. The time development of the wave at $\omega = 2\omega_0$ shows clear equiphase lines, and the wave seems to propagate in the composite with a negative v_{ph}. The electron plasma wave is enhanced more efficiently in the composite than in the overdense plasma because the second harmonic oscillation at every position causes the plasma oscillation.

We applied the STFFT to E_x and Fig. 8 shows the time development of frequency spectra of E_x at the same positions as in Fig. 6. The generation of the second harmonic wave $E_{x2\omega_0}$ is explained by Eq. (17). Equation (17) means that $E_{x2\omega_0}$ is derived from E_{z1} and B_{y1}. Both of them are electric and magnetic field of the radiated wave from the external current source and generation of $E_{x2\omega_0}$ starts at the arrival of E_{z1} and B_{y1}. According to Fig. 6, the wavefront of E_z includes some frequencies around ω_0, and it is predicted that the coupling between the wavefront and the component at ω_0 occurs by Eq. (17). Because frequencies of generated E_x seem to be determined as the frequencies of the wavefront $+\omega_0$ and the timing of generation of E_x seems to be derived from the arrival of the wavefront, we plot the white points shifted by ω_0 on Fig. 8 compared to Fig. 6.

A peak of the spectra at $\omega = 2\omega_0$ emerges when E_z at $\omega = \omega_0$ arrives at every position. The wave at $\omega = 2\omega_0$ is continuously generated after the arrival of E_z. The electron velocity v_z and the magnetic field B_y are calculated from

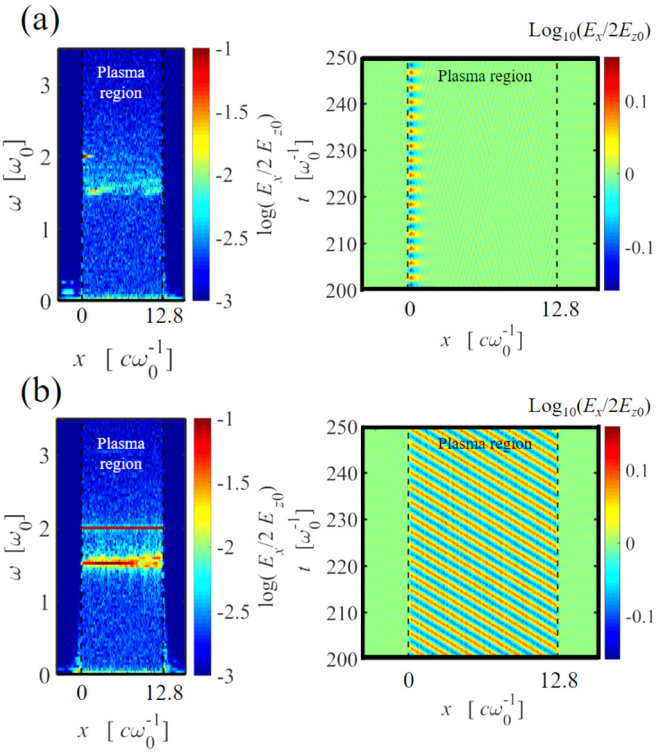

FIG. 7. Frequency spectra of E_x as a function of x and the time development of E_x at $\omega = 2\omega_0$ in $200 \le t \le 250$. The Fourier transform of E_x is performed over a period of $128 \le t \le 297.44$. (a) The overdense plasma and (b) the plasma-metamaterial composite where $J_{\mathrm{s}} = 2J_0$.

Eqs. (1) and (2), respectively, and both of them include the dispersion of the wavefront like E_z in Fig. 6. The Lorentz force includes many combinations of frequencies around $\omega = \omega_0$. The white points correspond to the spectra in $1.5\omega_0 < \omega \le 2\omega_0$ in Fig. 8.

A wave at $\omega = 1.5\omega_0$ includes components induced from the Lorentz force and from the electron plasma wave. The spectrum at $\omega = 1.5\omega_0$ can be observed before the arrival of E_z at $\omega = \omega_0$ at $x = 2.5$, and it emerges after the arrival at the other positions. These differences in the timing suggest that v_g of E_x at $\omega = 1.5\omega$ is smaller than that of E_z at $\omega = 0.5\omega_0$. The wave at $\omega = 1.5\omega_0$ is enhanced after mixing of the wave derived from the Lorentz force and the electron plasma wave, and it is observed continuously at all positions.

The spectra in $2\omega_0 < \omega < 2.5\omega_0$ are not observed in E_x though E_z includes the spectra in $\omega_0 < \omega < 1.5\omega_0$. According to Fig. 5(a), the waves in $\omega_0 < \omega < 1.5\omega_0$ has v_{g} greater than that at $\omega = \omega_0$, and the coupling between the waves in $\omega_0 < \omega < 1.5\omega_0$ and the wave at $\omega = \omega_0$ cannot occur because the waves in $\omega_0 < \omega < 1.5\omega_0$ go through before the wave at $\omega = \omega_0$ arrives at every position in the plasma region.

We applied the FFT to E_z and E_x in space and time in the plasma region when $J_{\mathrm{s}} = 2J_0$. Figure 9 shows the ω–k diagrams in the plasma region for E_z and E_x with and without the metamaterial. In the overdense plasma, $N(\omega_0)$ becomes a pure imaginary value and k becomes 0. The dotted line in Fig. 9(a-1) is the dispersion relation in the case without metamaterial and is expressed as $ck_{\mathrm{p}}(\omega) = \omega\sqrt{1-\omega_{\mathrm{pe}}^2/\omega^2}$.

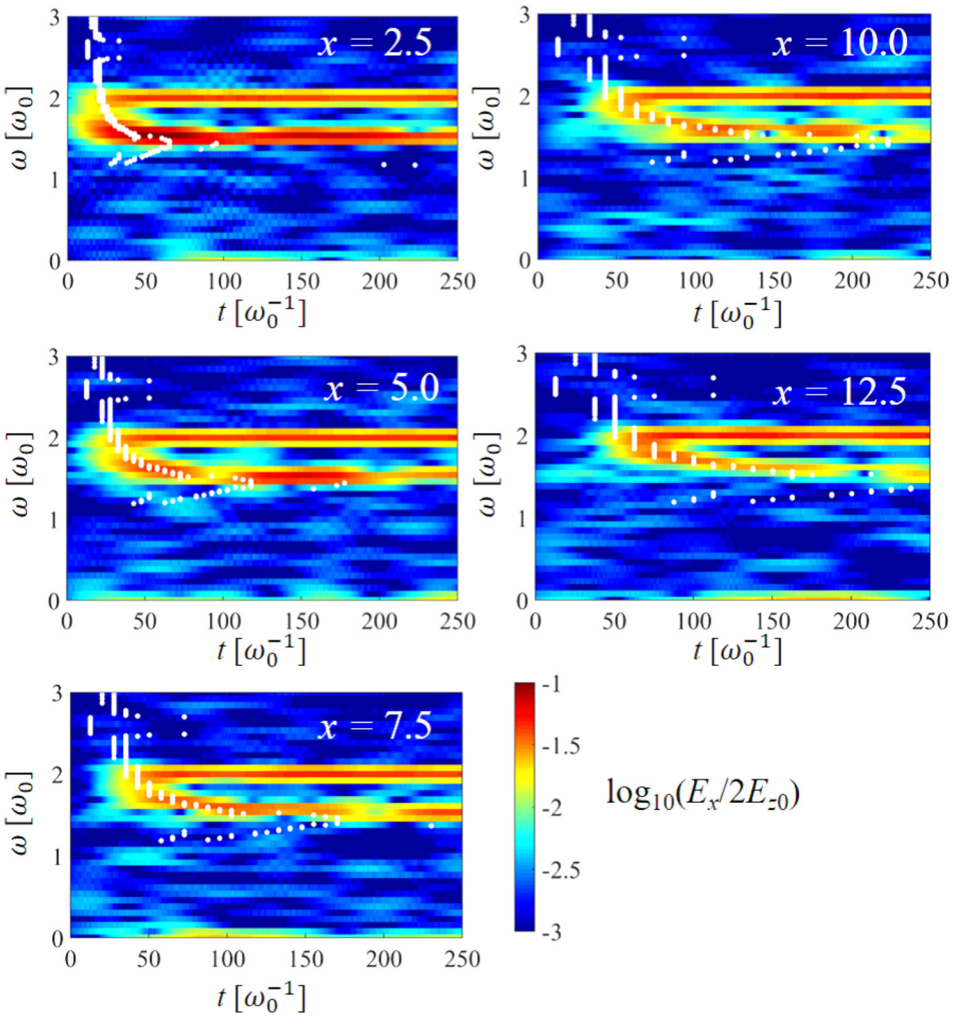

FIG. 8. The time development of the frequency spectra for the longitudinal component E_x from $x = 15$ to 25 when $J_s = 2J_0$. The white points indicate the calculated delay time.

In Fig. 9(a-1), the point with the maximum intensity exists at $(0, \omega_0)$, and a bright line emerges on $\omega = \omega_0$. In the overdense plasma, the evanescent wave is oscillating only in the limited area near the entrance and E_z becomes 0 in the downstream area beyond the skin depth in the plasma region. The resultant E_z comes to be similar to a pulse wave and the spectra of E_z in space include finite values of k around 0. The spectrum of $\omega = 1.5\omega_0$ exists at $(0, 1.5\omega_0)$ because this mode is the plasma oscillation derived from the kinetic motions of electrons at every position. It is a collective oscillation and behaves as a wave with the infinite wavelength.

Figure 9(a-2) shows the ω–k diagram of E_x in the overdense plasma. Spectra at $\omega = 2\omega_0$ are the same as them at $\omega = \omega_0$ in Fig. 9(a-1) because of the evanescent wave profile of E_x at $\omega = 2\omega_0$ in Fig. 7(a). The dotted line in Fig. 9(a-2) l_x is the electron plasma wave mode in the hot isotropic plasma expressed as $\omega^2 = \omega_{pe}^2 + 3v_{the}^2k^2$, and spectra in Fig. 9(a-2) show good agreement with l_x. The Lorentz force between v_x at $\omega = 2\omega_0$ and B_y at $\omega = \omega_0$ creates the third harmonic wave in the z-axis components. The third harmonic wave propagates in the overdense plasma because $3\omega_0 > \omega_{pe}$ and the working point exists at $(k_p(3\omega_0), 3\omega_0)$ in Fig. 9(a-1).

Figure 9(b-1) shows the ω–k diagram for E_z in the composite. The strong peaks are observed at $\omega = \omega_0$ and $\omega = 0.5\omega_0$ in E_z. The dotted line l_1 is the dispersion relation calculated using Eq. (7), and the working points for ω_0 and $0.5\omega_0$ exist on l_1. There are two peaks of ω_0 at $(-|k_{comp}(\omega_0)|, \omega_0)$ and $(|k_{comp}(\omega_0)|, \omega_0)$ where k_{comp} satisfies Eq. (7). The former indicates the propagating wave to the downstream side, and the latter indicates the reflection wave to the upstream side.

Figure 9(b-2) shows the ω–k diagram for E_x in the composite. The working point of $2\omega_0$ exists at $(-|2k_{comp}(\omega_0)|, 2\omega_0)$, and v_{ph} of the second harmonic wave is the same as that of E_z at $\omega = \omega_0$ in the composite. This point exists on l_0 and l_2 where l_0 is a line with v_{ph} being equal to that of the wave at $\omega = \omega_0$ in the composite. One of the dotted lines in Fig. 9(b-1) l_2 is moved from l_1 by $(-|k_{comp}(\omega_0)|, \omega_0)$ and expresses the coupling of waves on l_1 and the wave on $(-|k_{comp}(\omega_0)|, \omega_0)$. In Eq. (17) and Fig. 8, we showed the Lorentz force between v_z and B_y created E_x, and the coupling between waves with some frequencies and the wave at $\omega = \omega_0$ was mainly observed. Since l_2 indicates this coupling, spectra of E_x exist on l_2. The working point $(-|2k_{comp}(\omega_0)|, 2\omega_0)$ exists as an isolated point, and v_g at $\omega = 2\omega_0$ cannot be defined. This fact suggests that the second harmonic wave does not transfer electric energy in the composite unlike E_z at $\omega = \omega_0$. Phase matching should be satisfied in typical nonlinear optics and in second harmonic generation in negative N material in Ref. 13. Nevertheless, working points of second harmonic wave in ω-k diagram

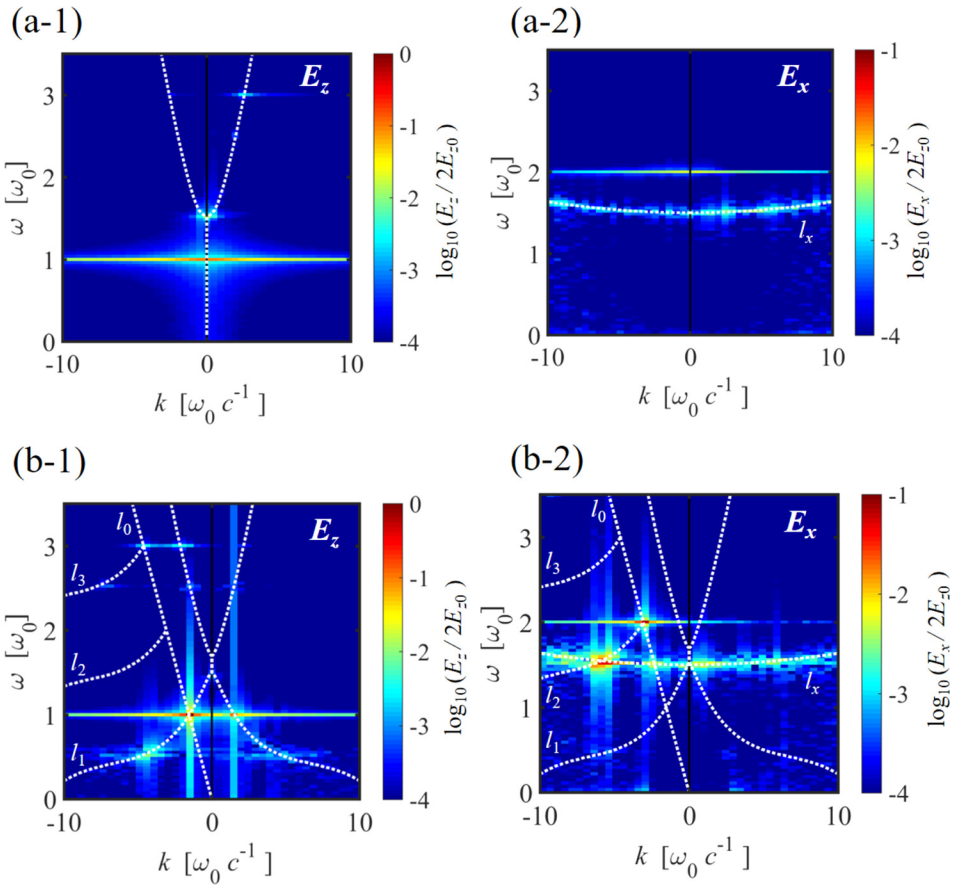

FIG. 9. The ω-k diagrams of the transverse wave E_z and the longitudinal wave E_x when $J_s = 2J_0$. (a-1) E_z and (a-2) E_x in the overdense plasma. (b-1) E_z and (b-2) E_x in the plasma-metamaterial composite. The line l_0 is the extended line between the origin and the point $(-|k_{comp}(\omega_0)|, \omega_0)$ where k_{comp} satisfies Eq. (7). The dispersion curve l_1 expresses the relation between k_{comp} and ω. The modes l_2 and l_3 are moved from l_1, and they are on the points $(-2|k_{comp}(\omega_0)|, 2\omega_0)$ and $(-3|k_{comp}(\omega_0)|, 3\omega_0)$, respectively.

should be on the dispersion curve, and the working point $(-|2k_{comp}(\omega_0)|, 2\omega_0)$ is isolated and exists far from the dispersion curve. Since generation of second harmonic waves in the composite in this simulation is derived from Lorentz force, we can observe the unique phase matching unlike the description in Ref. 13.

In the composite, E_z and B_y at $\omega = \omega_0$ propagate with satisfying the Maxwell equations, and they have $\pi/2$ phase difference in space and time from each other, but have the completely same v_{ph} and v_g. The transverse velocity of electrons v_z is induced from Eq. (2), and v_z has $\pi/2$-phase difference in space and π-phase difference in time from B_y. The second harmonic oscillation of electrons are induced at the individual positions, and the phase difference between positions moves upstream with v_{ph} of B_y. The resultant second harmonic wave is seen as the propagating wave with the negative N, though it is a longitudinal wave.

In Fig. 8, E_x at $\omega = 1.5\omega_0$ is enhanced after the arrival of E_z at $\omega = 0.5\omega_0$. The frequency falling in time in Fig. 8 is expressed as a shift of a working point on the line l_2 in Fig. 9(b-2). The working point starts from $(-|2k_{comp}(\omega_0)|, 2\omega_0)$ when the wavefront arrives. The point moves on l_2 to the lower frequency side, and the electron plasma wave starts to be enhanced when the point reaches the intersection of l_2 and the electron plasma wave mode l_x. The group velocity v_g on this point becomes a negative value, and the energy of the longitudinal wave is transferred upstream.

The third harmonic wave is found at two points; $(-|3k_{comp}(\omega_0)|, 3\omega_0)$ and $(-|k_{comp}(3\omega_0)|, 3\omega_0)$ in Fig. 9(b-1). The former is induced from the Lorentz force between v_x and B_y and this mode is seen on l_0 and l_3 as a propagating wave with v_{ph} of E_z at $\omega = \omega_0$ in the composite. The mode l_3 is moved from l_1 by $(-2|k_{comp}(\omega_0)|, 2\omega_0)$ and expresses the coupling of waves on l_2 and the wave on $(-|k_{comp}(\omega_0)|, \omega_0)$. The oscillation of electrons at $\omega = 3\omega_0$ radiates the electromagnetic wave, and this wave propagates in the composite with the wavenumber $-|k_{comp}(3\omega_0)|$.

We confirmed that the electromagnetic wave at $\omega = \omega_0$ propagated in the composite without the damping, and the second harmonic wave is generated all over the composite. If the composite works as a bulk material with the negative N, we can evaluate the efficiency of the generation of the second harmonic wave only with the macroscopic parameters ε and μ. This efficiency is equal to the susceptibility of the nonlinear optical materials.

3. Comparison with analytical model and particle simulations

We express the effective values of E_x at $\omega = 2\omega_0$ as $E_{x2\omega_0}$. Figure 10 shows the normalized $E_{x2\omega_0}$ with various intensities of J_s. When $J_s = rJ_0$ (r = 1, 2, 3, 4, and 5), the normalization factor is rE_{z0}. Figure 10(a) shows the case in the overdense plasma. The generation of the second harmonic wave occurs in the limited region up to $x \sim 2$ even if $J_s = 5J_0$ because the incident wave is the evanescent wave in the overdense plasma.

Figure 10(b) shows the normalized $E_{x2\omega_0}$ in the composite. The generation of the second harmonic wave occurs all over the composite, and the normalized intensity increases

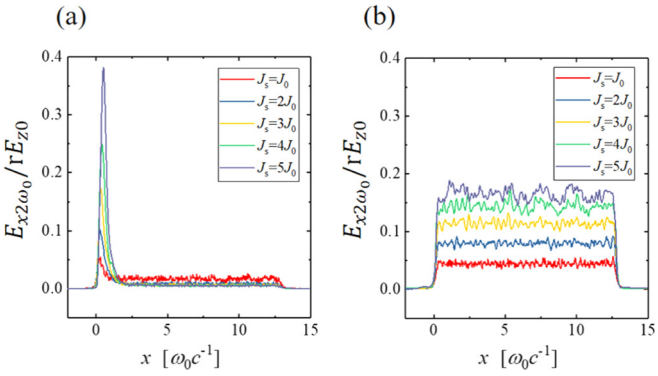

FIG. 10. The effective value of the longitudinal component E_x at $\omega = 2\omega_0$ when the input current $J_s = J_0$ to $5J_0$. (a) The overdense plasma. (b) The plasma-metamaterial composite. The constant r is the normalized amplitude of the input current $r = J_s/J_0$.

almost linearly as J_s increases up to $3J_0$. In the cases with strong input ($4J_0$ and $5J_0$), the normalized $E_{x2\omega_0}$ seems to approach the saturation level. According to the Gauss's law $\partial E_x/\partial x = \rho(x)/\varepsilon_0$, the strong E_x induces a spatial density ripple of electrons, and the reflection from the plasma region comes to be enhanced. The strong longitudinal wave works as the negative feedback for the generation of the second harmonic wave in the composite, and the normalized $E_{x2\omega_0}$ approaches the saturation level as the increment of J_s. The power efficiency of generation of the second harmonic waves in a magnetized dense plasma was reported as ~1% in Refs. 30 and 31. When $J_s > 3J_0$, the power efficiency becomes greater than 1% ($E_{x2\omega_0}/rE_{z0}$ becomes greater than 10%), and the efficiency is similar in comparison with that in the magnetized plasma.

Figure 11 shows the intensity of E_z at $x = 0$ as a function of ω_{pe} when the radiated wave enters the overdense plasma. In Fig. 11, $E_{z\max}$ is the maximum amplitude of the standing wave in the upstream side, and it becomes the double of the incident amplitude when the plasma works as the perfect reflector. The amplitude of E_z at the boundary decreases as ω_{pe} increases because the reflection coefficient from the overdense plasma is $e^{j\theta}$ and θ approaches π when ω_{pe}

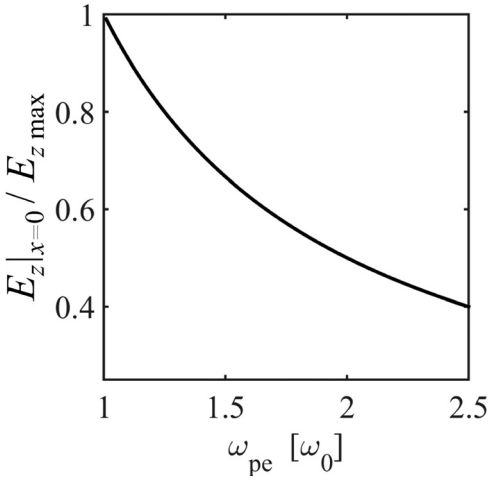

FIG. 11. The intensity of E_z at the boundary, $x = 0$, as a function of ω_{pe} in the case without a metamaterial. The intensity is normalized by the maximum amplitude of the standing wave $E_{z\max}$.

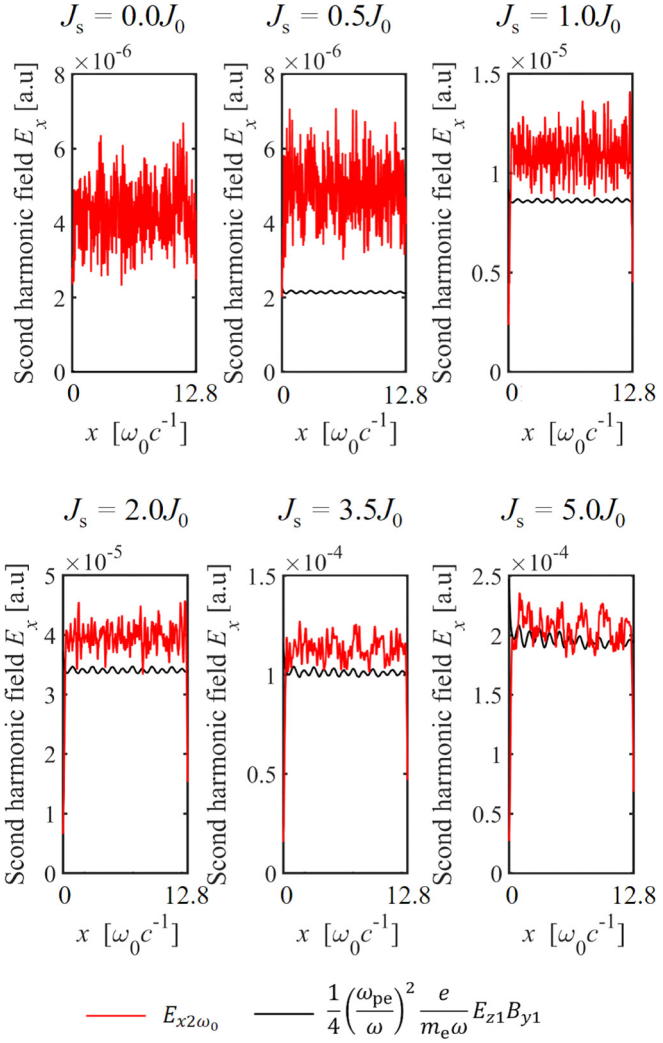

FIG. 12. Comparison between the effective values of $E_{x2\omega_0}$ in the simulation and the theoretical values given by Eq. (17). Red lines: Simulation, Black lines: Theory [Eq. (17)].

increases. The skin depth becomes short, and the intensity of the second harmonic wave cannot increase even if ω_{pe} increases.

In the case of the composite, the negative-μ metamaterial keeps the propagation of the electromagnetic wave even if ω_{pe} increases and we can obtain the efficient generation of the second harmonic wave. When n_e increases, the negative-μ metamaterial becomes more powerful in the generation of the second harmonic wave.

Figure 12 shows the comparisons between $E_{x2\omega_0}$ from the simulations and the theoretical intensity of the second harmonic wave from Eq. (17). The intensity of $E_{x2\omega_0}$ is not zero without the external current, and it is from the kinetic motions of electrons ($\sim 4 \times 10^{-6}$). When the external current has a finite value, $E_{x2\omega_0}$ shows good agreement with the sum of the theoretical intensity and the thermal noise. We confirm that Eq. (17) correctly expresses the intensity of the second harmonic wave. When the input current is strong, the spatial profile of $E_{x2\omega_0}$ includes a ripple unlike the profile by the theoretical calculation. Although we assume a constant ω_{pe} in Eq. (17), the strong input causes the density ripple and ω_{pe} has the spatial variation.

IV. CONCLUSION

We performed the one-dimensional particle simulation with the negative-μ metamaterial and simulated the propagation of the electromagnetic waves in the plasma-metamaterial composite. The electromagnetic wave propagating in the composite had the negative v_{ph} and the positive v_g. We calculated the dispersion relation of the composite including the kinetic effects of electrons and found the damping for transverse waves when N becomes large negative value. We found the efficient generation of the second harmonic longitudinal wave all over the composite because the transverse wave could propagate in the composite. We assumed that the composite has the macroscopic ε and μ and calculated the theoretical intensity of the second harmonic wave in the composite. We found that the theoretical intensity corresponded to E_x at $\omega = 2\omega_0$ and confirmed that the composite worked as the bulk material even if it consisted of the microscopic charged particles and the metamaterial with the macroscopic μ. These results strongly suggest that the combination of the plasma and the metamaterial can be the negative-N material, and the plasma can be a tunable component of metamaterials.

ACKNOWLEDGMENTS

This work was supported partly by a Grant-in-Aid for Scientific Research from the Japanese Ministry of Education, Culture, Sports, Science and Technology and a Grant-in-Aid for JSPS research Fellow.

[1]D. G. Swanson, *Plasma Waves*, 2nd ed. (IOP, London, 2003).
[2]R. F. Whitmer and E. B. Barrett, Phys. Rev. **121**, 661 (1961).
[3]R. R. Sharma and R. C. Sharma, J. Appl. Phys. **50**, 5655 (1979).
[4]S. C. Wilks, W. L. Kruer, and W. B. Mori, IEEE Trans. Plasma Sci. **21**, 120 (1993).
[5]V. Malka, A. Modena, Z. Najmudin, A. E. Dangor, C. E. Clayton, K. A. Marsh, C. Joshi, C. Danson, D. Neely, and F. N. Walsh, Phys. Plasmas **4**, 1127 (1997).
[6]M. A. Lieberman and A. J. Lichtenberg, *Principles of Plasma Discharges and Materials Processing* (Wiley, Hoboken, 1994).
[7]H. Sugai, I. Ghanashev, and M. Nagatsu, Plasma Sources Sci. Technol. **7**, 192 (1998).
[8]J. B. Pendry, A. J. Holden, D. J. Robbins, and W. J. Stewart, IEEE Trans. Microwave Theory Technol. **47**, 2075 (1999).
[9]V. G. Veselago, Sov. Phys. Usp. **10**, 509 (1968).
[10]R. W. Ziolkowski and E. Heyman, Phys. Rev. E **64**, 056625 (2001).
[11]S. Foteinopoulou, E. N. Economou, and C. M. Soukoulis, Phys. Rev. Lett. **90**, 107402 (2003).
[12]V. M. Agranovich, Y. R. Shen, R. H. Baughman, and A. A. Zakhidov, Phys. Rev. B **69**, 165112 (2004).
[13]I. V. Shadrivov, A. A. Zharov, and Y. S. Kivshar, J. Opt. Soc. Am. B **23**, 529 (2006).
[14]R. W. Boyd, *Nonlinear Optics*, 3rd ed. (Elsevier, London, 2008).
[15]R. A. Shelby, D. R. Smith, and S. Schultz, Science **292**, 77 (2001).
[16]A. A. Houck, J. B. Brock, and I. L. Chuang, Phys. Rev. Lett. **90**, 137401 (2003).
[17]C. G. Parazzoli, R. B. Greegor, K. Li, B. E. C. Koltenbah, and M. Tanielian, Phys. Rev. Lett. **90**, 107401 (2003).
[18]W. Rotman, IRE Trans. Antennas Propag. **10**, 82 (1962).
[19]Y. Nakamura and O. Sakai, Jpn. J. Appl. Phys., Part 1 **53**, 03DB04 (2014).
[20]A. Iwai, Y. Nakamura, A. Bambina, and O. Sakai, Appl. Phys. Express **8**, 056201 (2015).
[21]A. Iwai, Y. Nakamura, and O. Sakai, Phys. Rev. E **92**, 033105 (2015).
[22]O. Sakai, J. Appl. Phys. **109**, 084914 (2011).
[23]K. Kourtzanidis, D. M. Pederson, and L. L. Raja, J. Appl. Phys. **119**, 204904 (2016).
[24]Y. Omura and H. Matsumoto, "KEMPO1: Technical guide to one-dimensional electromagnetic particle code," *Computer Space Plasma Physics: Simulation Techniques and Softwares*, edited by H. Matsumoto and Y. Omura (Terra Scientific, Tokyo, 1993), pp. 21–65.
[25]Y. Omura, "One-dimensional electromagnetic particle code KEMPO1: A tutorial on microphysics in space plasmas," *Advanced Methods for Space Simulations*, edited by H. Usui and Y. Omura (TERAPUB, Tokyo, 2007).
[26]S. Yagitani, I. Nagano, Y. Omura, and H. Matsumoto, Radio Sci. **27**, 449, https://doi.org/10.1029/92RS00854 (1992).
[27]D. J. Bittencourt, *Fundamental of Plasma Physics*, 3rd ed. (Springer, New York, 2004).
[28]K. Grochenig, *Foundations of Time-Frequency Analysis* (Springer, Boston, 2001).
[29]S. K. Sinha and A. C. Sinha, Phys. Plasmas **3**, 59 (1996).
[30]P. Jha, R. K. Mishra, G. Raj, and A. K. Upadhyay, Phys. Plasmas **14**, 053107 (2007).
[31]M. Ghorbanalilu, Laser Part. Beams **30**, 291 (2012).